Instrument Science Report COS 2023-02(v1)

The G160M Spectral Resolution of the COS FUV Channel at Lifetime Position 6

Nathaniel E. B. Kerman[1], David Sahnow[1], Bethan James[1], Marc Rafelski[1], Kate Rowlands[1], Julia Roman-Duval[1], and Ravi Sankrit[1]

[1]Space Telescope Science Institute, Baltimore, MD

3 February 2023

ABSTRACT

We report on the COS instrument's FUV channel spectral resolution for observations using the G160M grating at Lifetime Position 6 (LP6). We compare measurements made on COS/FUV spectra taken with two central wavelength settings ("cenwaves" G160M/1533 and G160M/1623) to those predicted by an optical model of COS. We perform our validation by comparing ISM absorption lines found in the COS LP6 observations against the same lines found in high resolution STIS spectra after convolving them with the COS modeled line spread function (LSF). The models show that the COS G160M resolution at LP6 is generally within ±20% of its value at LP4. The resolution at most wavelengths and cenwaves falls between 10,000 and 16,000. The highest resolution attainable at LP6 is $R \sim$18,000, which is reached on the FUVA segment of G160M/1533.

Operated by the Association of Universities for Research in Astronomy, Inc., for the National Aeronautics and Space Administration.

Contents

1. Introduction

Starting with the advent of the Hubble Space Telescope's (HST's) Cycle 30 observations in October 2022, most routine COS/FUV observations with the G160M grating will utilize the sixth lifetime position (LP6) by default, rather than the previous G160M lifetime position, LP4 (James et al. 2022). This move will mitigate the effects of gain sag on the detector and enable COS to continue to provide sensitive UV capabilities to the astronomical community. LP changes affect the resolution of the instrument, both along the dispersion direction (the spectral resolution) and along the cross-dispersion direction (the spatial resolution). This instrument science report (ISR) describes the process followed to predict and validate the spectral resolution at LP6 while a separate ISR describes a similar process for the instrument's spatial resolution at LP6 (Kerman et al. 2023).

COS is affected by off-axis aberrations which reduce the spectral resolution of spectra taken as a function of their distance away from LP1 in the cross-dispersion direction. LP1, which was located along the instrument's optical axis, generally had the highest spectral resolution. At each subsequent lifetime position, the COS team develops models of the instrument Point Spread Function (PSF). These models are then validated using COS observations of interstellar medium absorption lines. In this ISR, we describe the observations and analyses used to validate the modeled resolution at LP6.

This spectral resolution analysis closely follows that described in the spectral resolution ISRs for LP2 (Roman-Duval et al. 2013), LP3 (Roman-Duval et al. 2017), and LP4 (Fox et al. 2018).

2. Optical Models

The COS team maintains an optical model of the COS instrument which utilizes CODE V software (https://www.synopsys.com/optical-solutions/codev.html) and is based on the original University of Colorado optical design of the instrument. A detailed description of the model can be found in Sahnow 2022. The model is used to generate two-dimensional PSFs for each of the grating and cenwave combinations, sampled at a range of wavelengths. Integrating the PSF for a given wavelength over the cross-dispersion direction (thus collapsing it onto the dispersion axis) yields the line spread function (LSF) at that wavelength. The LSF is then used to calculate the expected spectral resolution. Similarly, to obtain the cross-dispersion spread function (CDSF), the PSF is integrated in the orthogonal direction; this will be described in a separate ISR.

By taking into account the mid-frequency wavefront errors (MFWEs) on HST's primary and secondary mirrors, the optical model is able to properly characterize the non-gaussian wings of the COS LSF (Fox et al. 2018 and references therein). These wings contain a significant fraction of the total power in the PSF (up to 40%, depending on wavelength). The MFWEs arise from polishing errors on HST's primary and secondary mirrors (Ghavamian et al. 2009).

The COS PSFs are highly astigmatic, and light reaching the detector with an offset from the optical axis suffers from more aberrations than light at LP1 (Sahnow et al. 2013, Roman-Duval et al. 2013). Each Lifetime Position after the first (LP1) is offset from the COS optical axis and the aberrations affecting that LP increase with distance from LP1; LP6 is offset approximately +6.5 arcseconds from LP1. To partially compensate for these effects, the focus is changed for each LP and cenwave to minimize the width of the LSF and maximize the spectral resolution (Fox et al. 2018).

The COS FUV gratings are mounted on the Optics Select Mechanism 1 (OSM1), which rotates to move a grating/cenwave into place and also moves linearly to adjust the focus for the required observing mode. While the rotation depends only on the cenwave in use, the best focus of each cenwave also varies with LP. The total focus shift ($F_{\rm total}$) is the sum of shifts due to the linear ($F_{\rm linear}$) and rotational ($F_{\rm rotational}$) offets of the grating. To predict the LSF for each cenwave, the value of F_{total} and the grating tilt (α) must be input to the optical model.

As described in Roman-Duval et al. 2013, the grating tilt and total focus shift may be calculated using Equations 1 and 2, respectively.

$$\alpha = (N_{\rm R} - N_{\rm R0})\Delta R + \alpha_0 \tag{1}$$

$$F_{\rm total} = F_{\rm linear} + F_{\rm rotational} = (N_{\rm F} - N_{\rm F0})\Delta F - 42.8(N_{\rm R} - N_{\rm R0})\Delta F \tag{2}$$

Where, in the above equations:

- $N_{\rm R} - N_{\rm R0}$ is the number of rotation motor steps from nominal
- ΔR is the rotation step size (0.028125°)
- α_0 is the nominal grating tilt
- $N_{\rm F} - N_{\rm F0}$ is the number of linear focus motor steps from nominal
- ΔF is the linear focus motor step size (2.3518μm)

Table 1 tabulates the grating tilt for all cenwaves of G160M and is independent of LP. Table 2 gives the focus shifts of each such cenwave. The derivation of the best focus positions for LP6 is described in Fischer et al. 2022; these focus shifts are LP-dependent and each grating is indexed to its own nominal position. The OSM1 rotation and focus shift values in Tables 1 and 2 are specified in the `pcmech_OSMTbl` flight software table.

Once the LP6 grating tilt and total focus shift values were calculated and input to the optical model, the instrument's PSF was simulated for each cenwave on a grid of wavelengths covered by that cenwave; the spacing of this grid was 1 Å. Each PSF was then integrated over the cross dispersion axis, producing the LSF for that cenwave and wavelength. Figure 1 displays the profiles of LSFs sampled every 50 Å over 1350 to 1700 Å for cenwaves 1533 and 1623.

3. Observations

To analyze the spectral resolution at LP6, we obtained COS/FUV spectra of the star AV 75 taken at LP6 in program 16907 (PI Kerman). AV 75 is a blue supergiant star in the Small Magellanic Cloud with a sufficient UV brightness to allow for short, high signal-to-noise COS observations[1]. Its spectrum has been previously observed at high resolution by STIS and found to contain ISM absorption lines. This star was also used to verify the spectral resolution at LP2 through LP5. Only the G160M modes will be used at LP6 in Cycle 30 and we therefore only observed with the G160M grating. Following the precedent of the resolution analyses at LP2 (Roman-Duval et al. 2013), LP3 (Roman-Duval et al. 2017), LP4 (Fox et al. 2018), and LP5 (Dieterich et al. 2023), observations were obtained using only the extreme cenwaves of the grating. These cenwaves are those with the shortest and longest wavelengths, providing coverage of the entire wavelength range of the grating. For G160M, these are 1533 and 1623. Prior resolution analyses took place before the 1533 cenwave was commissioned, and therefore the extreme cenwaves in the previous LPs' spectral resolution analyses were

[1]AV 75 (also known as AzV 75) has magnitudes $U = 11.553$, $B = 12.604$, $V = 12.756$ and spectral type O5.5I(f) as cataloged by the SIMBAD Astronomical Database (Wenger et al. 2000, Massey et al. 2009, Bonanos et al. 2010).

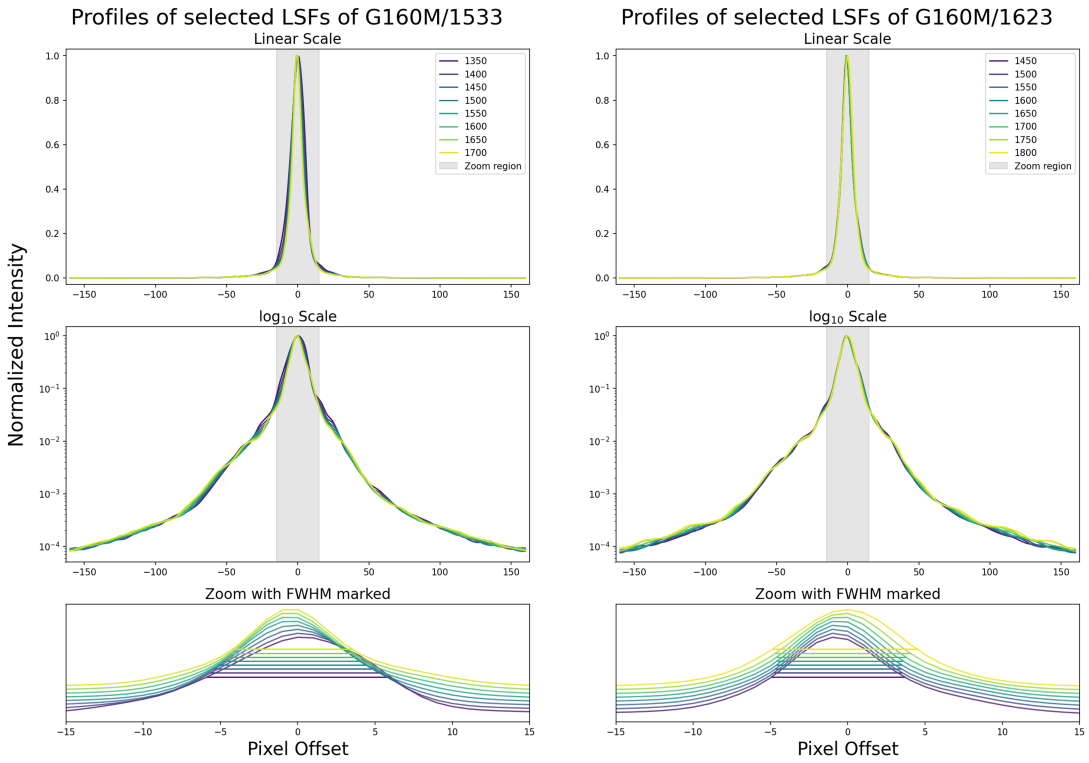

Figure 1. Normalized profiles of a range of modeled LSFs at different wavelengths (indicated by color) for cenwaves 1533 (**left**) and 1623 (**right**). For each cenwave, the **top** panel shows the linear-scale profile, while the **middle** panel shows the same information on a $\log_{10}$-scale. The **bottom** panel show a linear-scaled zoom of the LSF within the central 30 pixels. The LSF's full width at half maximum (FWHM) is marked with a horizontal line. The LSFs at different wavelengths are offset on the y-axis for clarity. This figure samples the LSF every 50 Å.

1577 and 1623. Exposure times of the observations were chosen to achieve a signal-to-noise ratio of 60 per resolution element at 1600 Å. Table 3 lists the COS observations obtained as part of program 16907.

In addition to the COS observations, we utilized an existing STIS E140M spectrum of AV 75 which was processed and made available in the Ultraviolet Legacy Library of Young Stars as Essential Standards (ULLYSES) project's fifth data release of high level science products (Roman-Duval et al. 2020)[2]. This spectrum was produced by combining STIS E140M echelle grating spectra of AV 75 from datasets `o4wr11010` and `o4wr11020`, both obtained as part of HST program 7437 (PI D. Lennon).

[2]The ULLYSES high level science products can be found at https://ullyses.stsci.edu/ullyses-latest-dr.html.

Table 1. The grating tilt values for the COS FUV modes discussed in this ISR. These values are LP-independent.

Grating	Cenwave	Rotation Position $N_{\rm R}$ (motor steps)	Steps from nominal $N_{\rm R} - N_{\rm R0}$ (motor steps)	Grating Tilt α (degrees)	Rot. Foc. Shift $F_{\rm rot}$ (mm)
G160M	1533	11218	$+23$	-19.4531	2.315
G160M	1577	11203	$+8$	-19.8750	0.805
G160M	1589	11199	$+4$	-19.9875	0.403
G160M	1600	11195	0	-20.1000	0.000
G160M	1611	11191	-4	-20.2125	-0.403
G160M	1623	11187	-8	-20.3250	-0.805

Table 2. Focus offsets for COS FUV modes at LP6, as used in the optical model.

Grating	Cenwave	Rot. Foc. Shift $F_{\rm rot}$ (mm)	Foc. Position N_F (motor steps)	Steps from nominal $N_F - N_{F0}$ (motor steps)	Lin. Foc. Shift $F_{\rm lin}$ (mm)	Tot. Foc. Shift $F_{\rm tot}$ (mm)
G160M	1533	$+2.315$	-770	-726	$+1.707$	$+4.023$
G160M	1577	$+0.805$	-232	-188	$+0.442$	$+1.247$
G160M	1589	$+0.403$	-62	-18	$+0.042$	$+0.445$
G160M	1600	0.000	$+108$	$+152$	-0.357	-0.357
G160M	1611	-0.403	$+278$	$+322$	-0.757	-1.160
G160M	1623	-0.805	$+448$	$+492$	-1.157	-1.962

Table 3. Observations used in the LP6 spectral resolution program.

Setting	Prog. ID	Date (UT)	Exposure Time[a] (s)	Dataset ID
G160M/1533	16907	2022-03-10	2076	`letc01010`
G160M/1623	16907	2022-03-10	1668	`letc01020`

[a]Total exposure time combined across all four FP-POS positions.

4. Analysis

We followed the analysis procedure used by Fox et al. (2018) to validate the spectral resolution at LP4. By comparing each LP6 cenwave's COS spectrum to a much higher resolution STIS reference spectrum ($R = 45,800$; Prichard et al. 2022), the modeled effects of the COS LSF can be verified against the observed effects. The observed spectrum is modeled by the high-resolution STIS spectrum convolved with the COS model LSF.

The full analysis procedure (repeated for each cenwave) is described below:

1. We obtained raw COS data from HST program 16907 from the MAST archive, which consist of COS LP6 spectra of the star AV 75 (the datasets are shown in Table 3). We calibrated this data with CalCOS (version 3.4.3) and the reference files created for use at LP6 [3].

2. We identified interstellar medium (ISM) absorption lines in the COS spectrum.

   - ISM absorption lines are required because, unlike other lines in the star's spectrum, they are not formed in the stellar atmosphere or wind. As such, they do not have as complex a structure (e.g., from wind kinematics or stellar rotation), nor are they as variable as the lines which originate in the star. The lack of variability is important since the STIS spectra were not obtained concurrently.
   - There are very few ISM absorption lines in the wavelength range of the G160M grating, but one or two were found on each detector segment for both cenwave 1533 and 1623. The lines were of different optical depths and most were multiplets, which can reduce the reliability of this analysis. Lines with a higher optical depth (but not saturated) and without blending are more favorable for this analysis.
   - For the purposes of this ISR, a line which reduced the flux to less than 20% of the surrounding continuum was considered a "strong" line. Those which reduced flux to between 20-50% of the continuum were considered "weak" lines and those which reduced flux to between 50-80% were considered "very weak" lines. This classification was used to create a weighted average of the resolutions measured in each spectral feature to estimate the overall resolution for a cenwave (Step 7).

3. We generated a grid of degraded and enhanced variations of the modeled LSF by widening or narrowing it following the method described in Fox et al. 2018. Beginning with the predicted LSF output by the optical model, the LSF with the most degraded resolution had its full width at half maximum (FWHM) increased

[3]The reference files used are accessible via the HST Calibration Reference Data System (CRDS) website under the observatory context: `hst_1036.pmap`.

by 50%, and the LSF with the most enhanced resolution had its FWHM decreased by 50% compared to the unaltered model. The grid was sampled at increments of 5% changes to the FWHM. In the case of the degraded LSFs, as the FWHM was increased, the resolution proportionately decreased. For the enhanced LSFs, the FWHM was reduced and the resolving power was instead increased. The LSF in the center of the grid was the unchanged LSF produced by the optical model.

4. We obtained a high resolution STIS spectrum from the ULLYSES database (see Section 3). We then convolved the STIS spectrum with each of the LSFs in the grid to produce a second grid, consisting of convolved STIS spectra.

5. For each ISM line found in the COS spectrum, we determined the convolution that best reproduced the COS LP6 spectrum. This was done using a χ^2 analysis to minimize the residuals between the COS and convolved STIS spectrum within a narrow spectral window around the ISM line. A version of the same code employed for the LP4 analysis was used for LP6. This step generated Figures 2 (cenwave 1533) and 3 (1623) which show both the analyzed wavelength regions of the spectra (left panels) and the χ^2 analysis for each ISM line (right panels). The dashed vertical lines indicate the windows around each ISM line used for the χ^2 analysis.

6. The version of the modeled LSF used to create the best-fit convolution was determined to be the best-fit LSF. Its FWHM was measured and used to calculate a best-fit resolving power for each ISM line as in Equation 3,

$$R_{\rm line} = \frac{\lambda}{\Delta\lambda} \tag{3}$$

   where λ is the wavelength of the line and $\Delta\lambda$ is the FWHM of the best-fit LSF.

7. The best-fit resolution for each ISM line was compared against the optical model's predicted resolution at the same cenwave and wavelength to assess their equivalence. This step generated Figures 4 (cenwave 1533) and 5 (1623), which show the modeled and measured resolutions as a function of wavelength.

8. The figures from the previous step were then examined to determine whether the observations validated the model, i.e. if they were within the $\sim$20% tolerance accepted by the LP4 spectral resolution analysis specified in Fox et al. 2018.

Additional figures were then constructed to display the LP6 resolution. Figure 6 presents the model's resolution across all wavelengths of all LP6 cenwaves. Figure 7 then presents this LP6 resolution as a percentage of the model's LP4 resolution.

We also generated and include Figures 8 and 9 in this report. For cenwaves 1533/1577 and 1623, respectively, these figures present regions of the COS spectrum of AV 75 taken at LP4 and LP6 as well as the STIS spectrum convolved with the COS

Table 4. Percent differences between the observed and model LSF FWHM for both the LP4 and LP6 analyses, calculated as $100 \times \frac{\mathrm{FWHM_{observed}} - \mathrm{FWHM_{modeled}}}{\mathrm{FWHM_{modeled}}}$. Differences are measured at each ISM line. The lines used are different for the LP4 and LP6 analyses.

LP4		**LP6**	
ISM line	Difference	ISM line	Difference
cenwave at wavelength on segment	%	*cenwave at wavelength on segment*	%
1577 at 1527 Å on FUVB	+5	1533 at 1370 Å on FUVB	+10
1577 at 1609 Å on FUVA	+20	1533 at 1394 Å on FUVB	−10
1577 at 1657 Å on FUVA	+25	1533 at 1609 Å on FUVA	+30
1623 at 1527 Å on FUVB	−5	1533 at 1657 Å on FUVA	+15
1623 at 1609 Å on FUVB	+5	1623 at 1527 Å on FUVB	+5
		1623 at 1657 Å on FUVA	5

LSF. These figures demonstrate visually the differences in performance between LP4 and LP6.

5. Results and Conclusions

Based on the measurement of spectral resolution with six ISM lines across cenwaves 1533 and 1623, we have verified the spectral resolution predicted by the optical model for all COS/FUV modes at LP6. Figure 6 shows the validated model resolutions for all G160M cenwaves moving to LP6. Resolution generally increases with wavelength. For all cenwaves except 1533, this trend reverses at the longest wavelengths (∼1750 Å). All cenwaves except for 1533 follow a very similar pattern in Figure 6. Cenwave 1533 was expected to have some differences in behavior from the other G160M cenwaves given its larger offset in wavelength, focus, and tilt from the longer cenwaves, and the fact that its relative focus was not measured before launch.

The lack of strong, isolated absorption lines in the wavelength range of G160M limits the accuracy to which we can measure the spectral resolution. As such, we instead seek only to *validate* the model's predicted resolution by showing the measured resolutions are consistent with the model. Generally, the resolution measured using each ISM line is within ±15% of the predicted resolution. However, in the case of the multiplet line around 1609 Å (panel 3 of Figure 2) the measured resolution differs from the predicted resolution by ∼30%.

Table 4 presents the differences between the model and observed FWHM at each ISM line measured in the LP4 and LP6 analyses. This table demonstrates that the agreement between the model and observations is comparable between the LPs.

As shown in Figure 7, the modeled resolution at LP6 is generally $0 - 20\%$ lower than that for LP4. However, on the FUVA segment of cenwave 1533 and the FUVB segment of 1623, the LP6 modeled resolution is higher than that of LP4 by up to ∼15% and ∼5%, respectively. Cenwaves 1577 and 1589 were the most used G160M cenwaves in HST Cycle 29. Each of these workhorse cenwaves has an LP6 resolution roughly

$85 - 90\%$ that of LP4.

Acknowledgements

Nathaniel Kerman acknowledges the contributions of Andrew Fox and Sergio Dieterich, whose work on the LP4 and LP5 programs helped the author orient himself in this analysis. Additionally, Mr. Kerman thanks the other COS team members who contributed to the `IDL` resolution analysis code used to measure the observed resolution and those who provided input to improve this report.

Change History for COS ISR 2023-02

Version 1: 3 February 2023 – Original Document

References

Bonanos, A. Z. et al. 2010, Astron. J., 140, 416-429, "Spitzer SAGE-SMC infrared photometry of massive stars in the Small Magellanic Cloud"

Dieterich, S. et al. 2023, COS ISR 2023-XX, "The Spectral Resolution of the COS FUV Channel at Lifetime Position 5"

Fischer, T. et al. 2022, COS ISR 2022-12, "Exploring the Focus of New COS FUV Lifetime Positions: G130M/1222 and G160M at LP6"

Fox, A., et al. 2018, COS ISR 2018-07, "The Spectral Resolution of the COS FUV channel at Lifetime Position 4"

Ghavamian, P., et al. 2009, COS ISR 2009-01, "Preliminary Characterization of the Post-Launch Line Spread Function of COS"

James, B. L., et al. 2022, COS Instrument Handbook, "Cosmic Origins Spectrograph Instrument Handbook (Version 14.0)"

Kerman, N. et al. 2022, COS ISR 2023-XX, "The Spatial Resolution of the COS FUV channel at Lifetime Position 6"

Massey, P. et al. 2009, Astrophys. J., 692, 618-652, "The physical properties and effective temperature scale of O-type stars as a function of metallicity. III. More results from the Magellanic clouds"

Prichard, L., et al. 2022, STIS Instrument Handbook, "Space Telescope Imaging Spectrograph Instrument Handbook for Cycle 30 (Version 21.0)"

Roman-Duval, J., et al. 2013, COS ISR 2013-07, "COS/FUV Spectral and Spatial Resolution at the new Lifetime Position"

Roman-Duval, J., et al. 2017, COS ISR 2017-06, "Spectral Resolution of COS/FUV at Lifetime Position 3"

Roman-Duval, J., et al. 2020, Research Notes of the AAS, "Ultraviolet Legacy Library of Young Stars as Essential Standards (ULLYSES): Data Release I"

Sahnow, D., et al. 2013, COS ISR 2013-13, “COS/FUV Characterization of Optical Effects at Potential Lifetime Positions”

Sahnow, D. 2022, Proceedings of the SPIE 12181, “Optical modeling of new lifetime positions for the Cosmic Origins Spectrograph (COS)”

Wenger, M., et al. 2000, Astron. Astrophys. Suppl. Vol. 143, p. 9–22, “The SIMBAD astronomical database. The CDS reference database for astronomical objects”. (*Version: SIMBAD4 1.8 - 2022-08*)

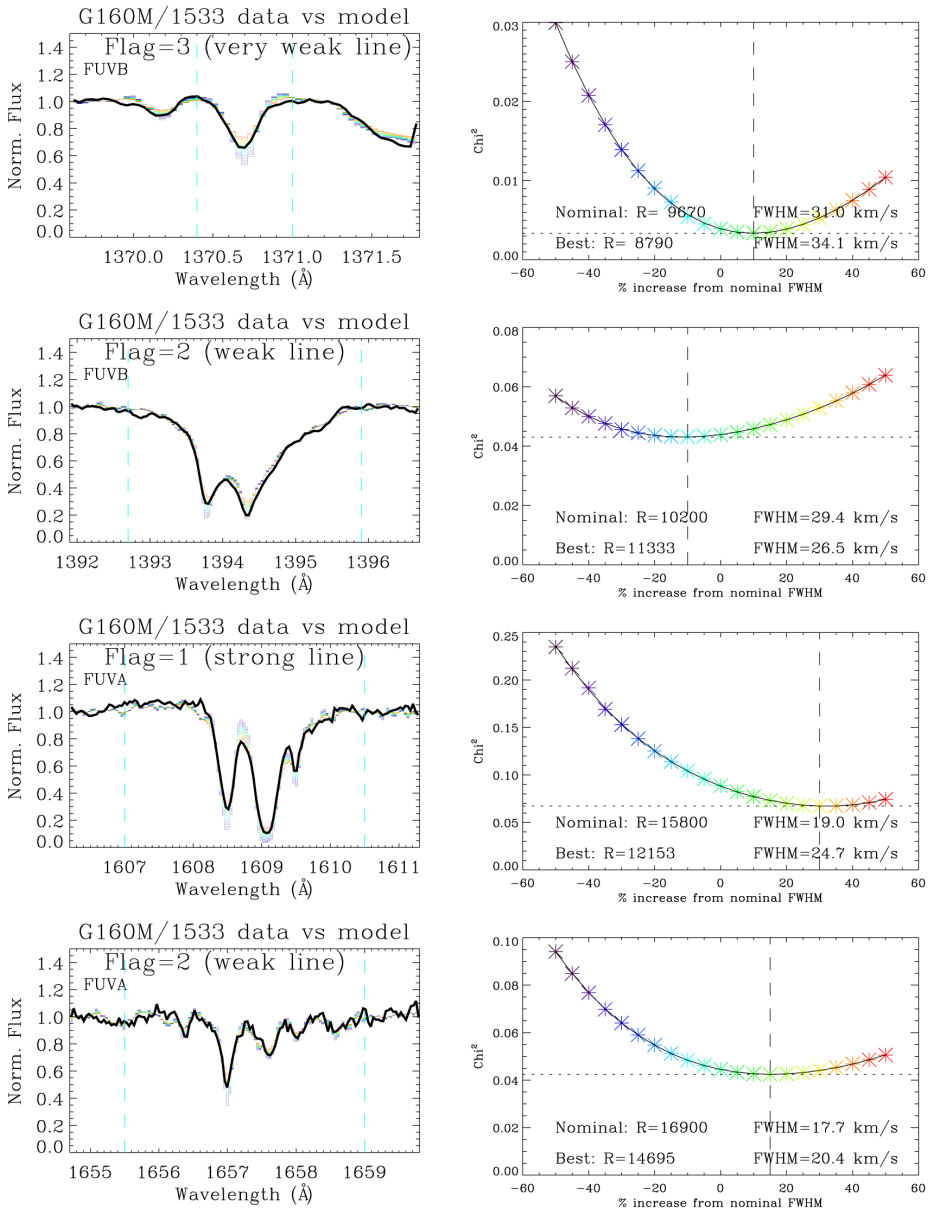

Figure 2. For each ISM line identified in the COS LP6 1533 spectrum for which the spectral resolution was calculated, the **lefthand side** shows a comparison of the COS spectrum (black) with the STIS spectrum convolved with enhanced and degraded COS LP6 model LSFs (rainbow colors). The flux is normalized to the continuum regions. The spectral windows on which the χ^2 analysis was performed are indicated with dashed blue lines. The **righthand side** shows the χ^2 analysis described in Step 5: the χ^2 value of each convolution is plotted on the y axis against the percent by which the FWHM of the LSF used has been increased or reduced relative to the nominal LSF predicted by the optical model . This is also the percentage which the measured resolution is reduced relative to the model. The minimum χ^2 is marked, indicating the best-fit LSF, whose resolution is noted as "Best".

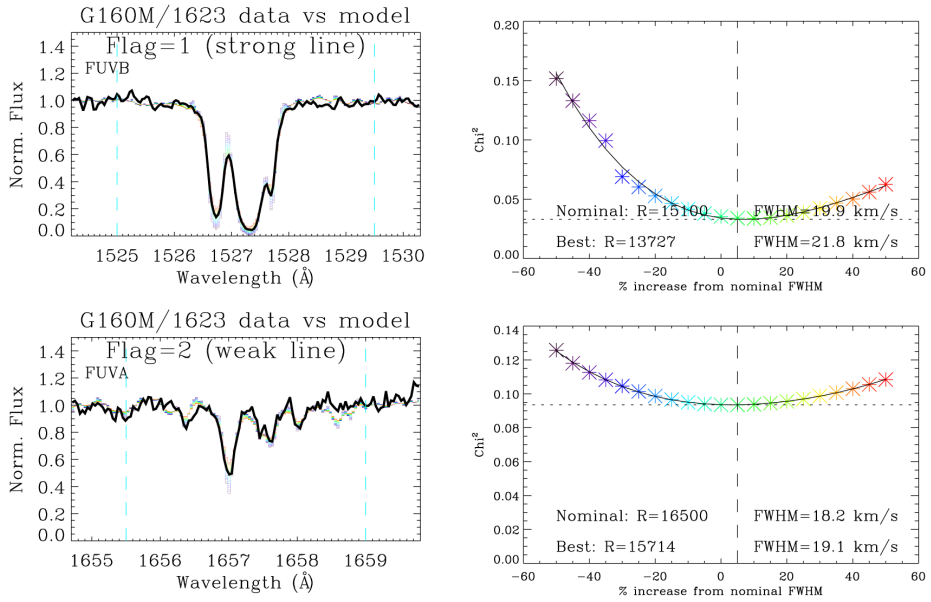

Figure 3. Same as Figure 2, except analyzing G160M/1623 instead of G160M/1533.

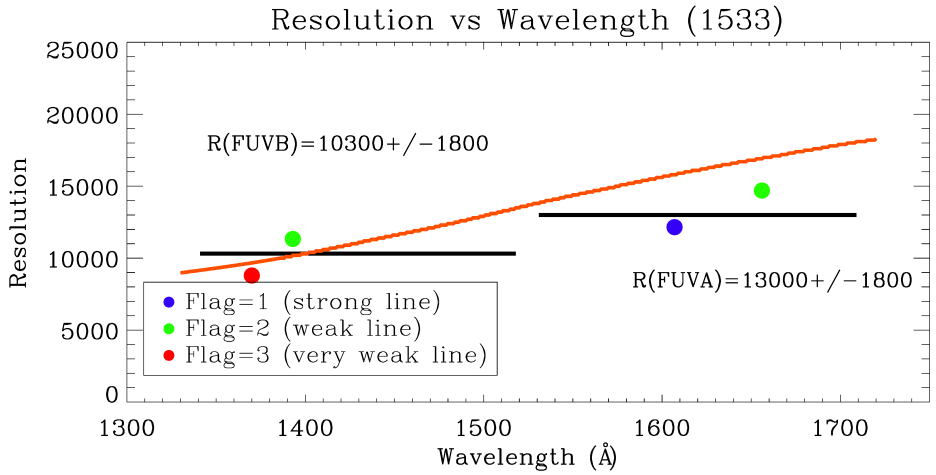

Figure 4. Resolution as a function of wavelength for G160M/1533. The red line is the resolution predicted by the optical model. The points show the experimental resolution measured at individual ISM absorption lines. The black lines represent the average measured resolution for FUV segment A (**right**) and B (**left**), inversely weighted by the flag number shown on the plot. The weighted mean resolution value for each segment ± the spread of individual measurements on that segment is also noted on the plot.

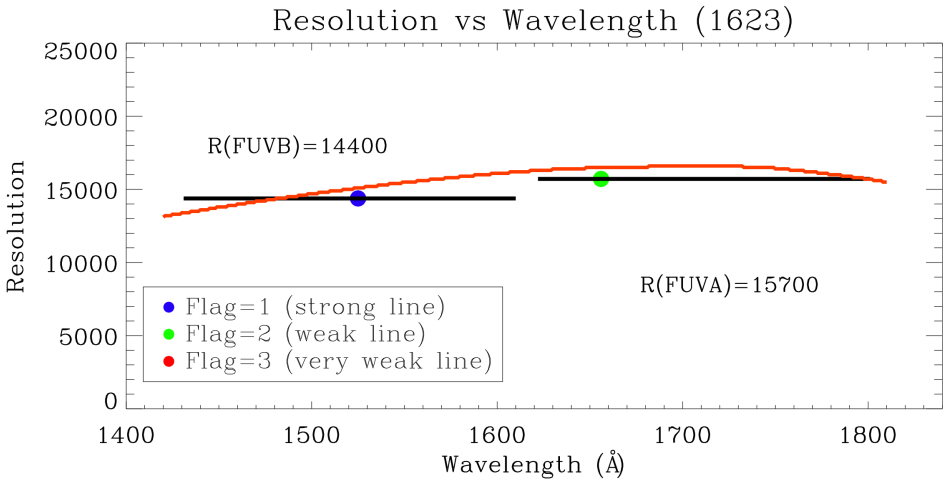

Figure 5. Same as Figure 4 for G160M/1623. Because only one ISM line was found on each segment, no spread in resolution is noted.

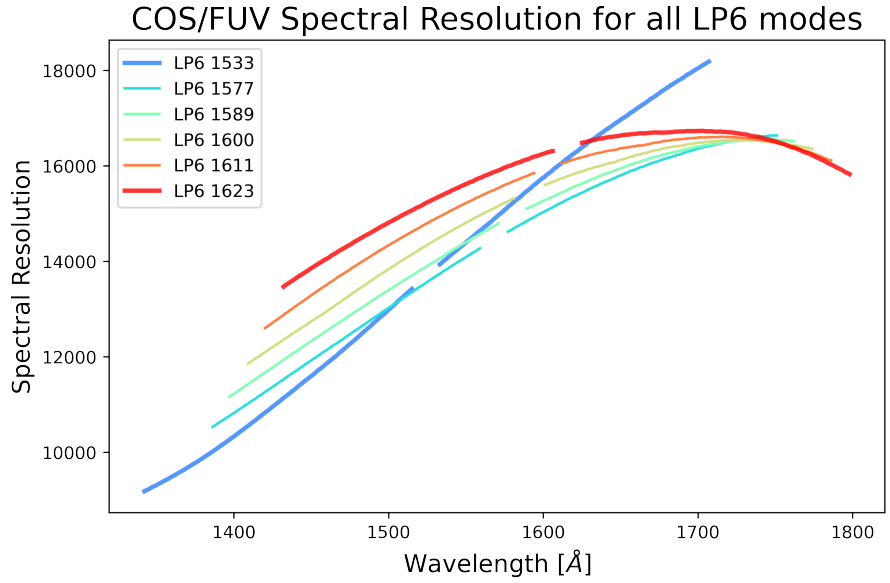

Figure 6. The optical model's predicted spectral resolution as a function of wavelength for all COS G160M cenwaves moving to LP6. The extreme cenwaves (1533 and 1623) whose models were directly verified are indicated with thicker lines (darker blue and red, respectively).

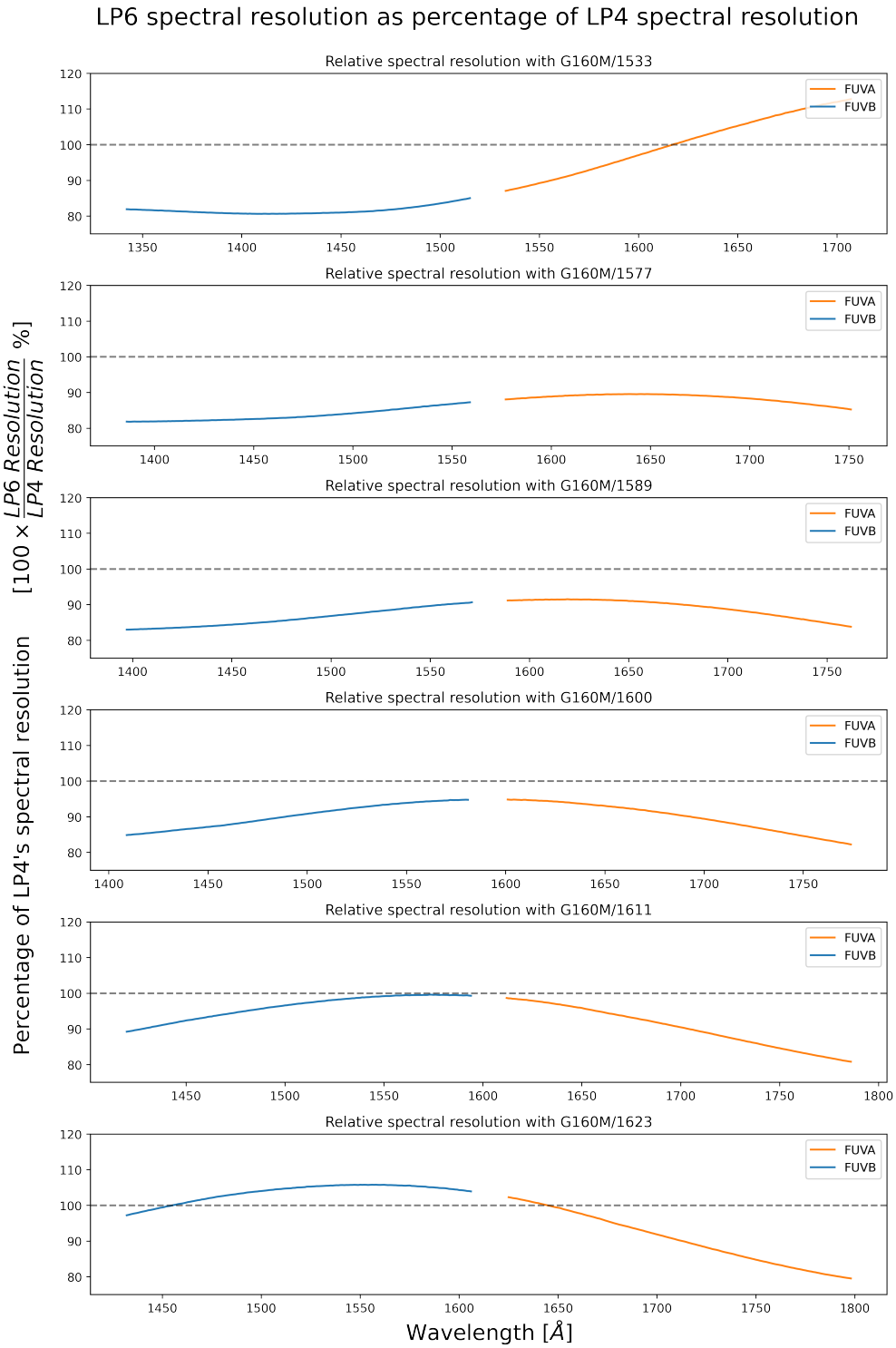

Figure 7. Relative modeled spectral resolution for all COS G160M cenwaves moving to LP6 as a percentage of LP4 resolution and plotted against wavelength. The dashed line indicates 100% of the LP4 resolution.

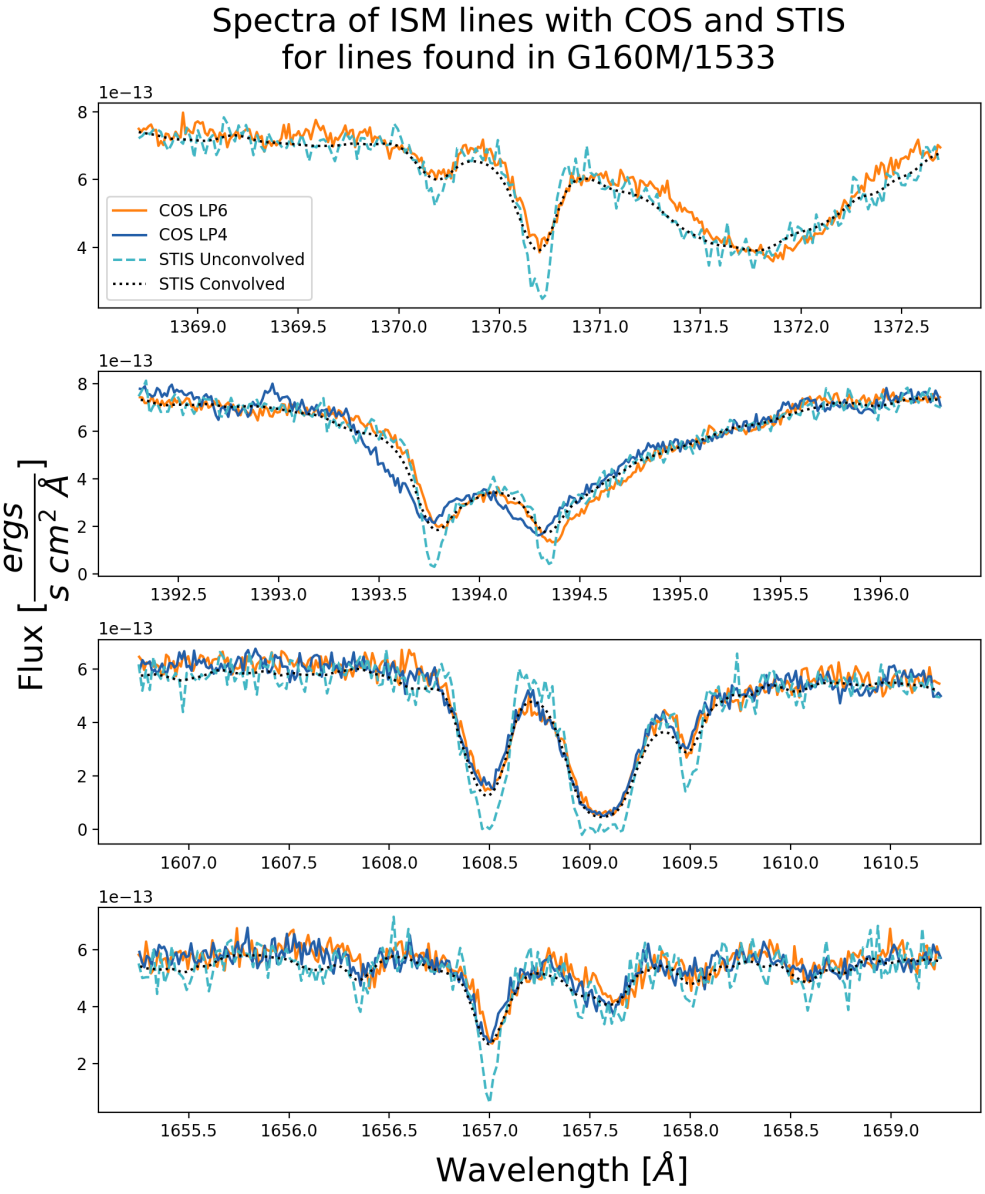

Figure 8. Comparison of COS LP4 G160M/1577 (blue) and LP6 G160M/1533 (orange) spectra of ISM lines in AV 75. While LP6's short cenwave spectrum was taken with cenwave 1533, the LP4 program took data with 1577, making the comparison indirect. Additionally cenwave 1577's wavelength range is shifted higher than 1533's, so there is no LP4 data in the top panel at ∼1370Å. The high resolution STIS spectrum is also shown, both before (dashed cyan) and after (dotted black) convolution with the COS LP6 LSF.

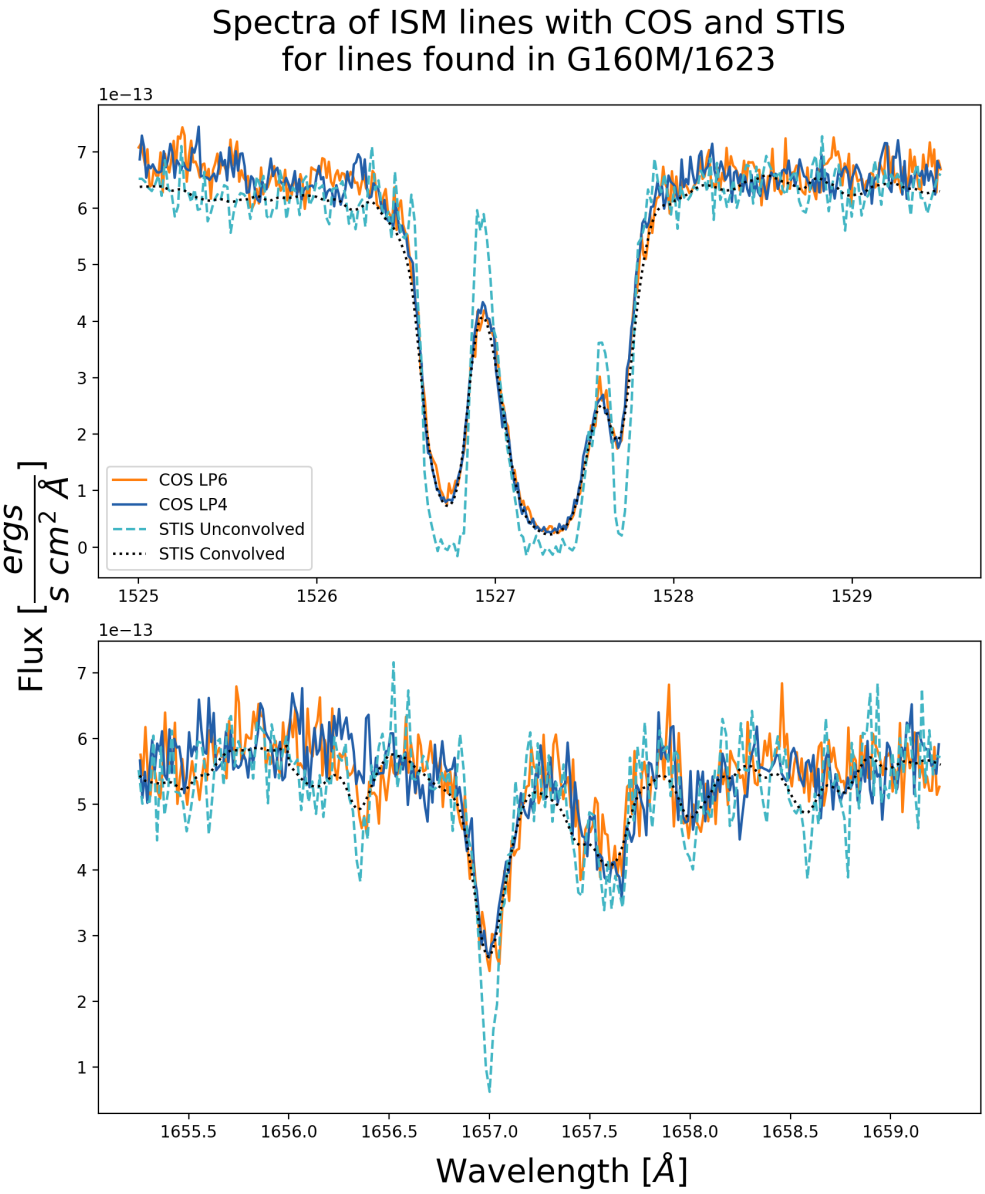

Figure 9. Same as Figure 8, except both LP4 and LP6 COS spectra were taken with G160M/1623, making the comparison more direct. Consistent with the predicted change in spectral resolution shown in Figure 7, there is little difference between the LP4 and LP6 spectra observed with cenwave 1623 at 1527 Å and 1657 Å.